Study of the $^{32}S(^{3}He,d)^{33}Cl$ one-proton transfer reaction with a new generation hodoscope

IOP Conf. Series: Journal of Physics: Conf. Series **1308** (2019) 012007 doi:10.1088/1742-6596/1308/1/012007

Study of the ^{32}S(^{3}He,d)^{33}Cl one-proton transfer reaction with a new generation hodoscope

M Cinausero[1], D Dell'Aquila[2], I Lombardo[2], M Vigilante[3,4], S Barlini[5], R Bolzonella[10,1], M Bruno[6,7], A Buccola[8,5], S Cartuan[1], G Casini[5], M Cicerchia[10,1], M D'Andrea[2], M Degerlier[12], D Fabris[9], L Gasques[11], F Gramegna[1], A Lepine-Szily[11], G Mantovani[10,1], T Marchi[1], S Piantelli[5], V Rigato[1], L Scomparin[10,1] and S Valdrè[5]

[1] INFN-Laboratori Nazionali di Legnaro, Legnaro, Italy
[2] INFN-Sezione di Catania, Catania, Italy
[3] Università degli Studi di Napoli "Federico II", Napoli, Italy
[4] INFN-Sezione di Napoli, Napoli, Italy
[5] INFN-Sezione di Firenze, Firenze, Italy
[6] Università degli Studi di Bologna, Bologna, Italy
[7] INFN-Sezione di Bologna, Bologna, Italy
[8] Università degli Studi di Firenze, Firenze, Italy
[9] INFN-Sezione di Padova, Padova, Italy
[10] Università degli Studi di Padova, Padova, Italy
[11] Instituto de Fisica da Universidade de São Paulo, 05508-090 São Paulo, Brasil
[12] Science and Art Faculty, Physics Department, Nevsehir Haci Bektas Veli Univ., Nevsehir, Turkey

E-mail: dellaquila.daniele@gmail.com

Abstract. The ^{32}S(^{3}He,d)^{33}Cl one-proton transfer reaction is a powerful tool to investigate the spectroscopy of low-lying states in the proton-rich ^{33}Cl nucleus. However, the extraction of firm differential cross-section data at various angles, against which benchmarking theoretical models to correctly constrain the spectroscopy of ^{33}Cl, is made challenging by the presence of competitive reaction products contaminating the detected energy spectra. We have recently measured the ^{32}S(^{3}He,d)^{33}Cl reaction at 9.8 MeV incident energy by using a new generation hodoscope of silicon detectors, capable to detect and identify emitted deuterons down to energies of the order of 2 MeV. The high angular segmentation of our hodoscope allowed to unambiguously disentangle the contribution of one-proton transfer reactions in the ground state of ^{33}Cl and in its 0.810 MeV, 2.352 MeV, 2.685 MeV, 2.846 MeV excited states from contaminant deuteron-emitting reactions. These data will be crucial to help to constrain J^{π} and spectroscopic factor C^2S_p values of low-lying ^{33}Cl states, still ambiguous in the literature. The present status of the analysis is discussed in the paper.

1. Introduction

Nuclear reactions at low and intermediate energies allow to probe many properties of nuclear systems and their governing forces such as the structure of nuclei [1, 2, 3, 4] and clustering phenomena [5, 6, 7], their influence in Astrophysics [8], the dynamics of nucleus-nucleus collisions [9, 10, 11], and their interplay [12]. While the latter requires often the use of 4π detectors [13, 14, 15] because of the complexity of the final state of the collisions, nuclear spectroscopy

studies are typically more selective, enabling the use of more compact devices [16]. In this framework, transfer reactions are a class of particularly selective processes that allow to explore specific degrees of freedom in nuclear systems such as single-particle configurations. In the literature, several transfer reaction studies have been performed by using spectrometers like MAGNEX at INFN-LNS [17], VAMOS at GANIL [18] and K600 at iThemba LABS [19]. Recently, new high-resolution and modular detectors for nuclear physics have been developed (see, for example FARCOS at INFN-LNS [20] or HiRA10 at MSU-NSCL [21]) to be used for nuclear reactions or as ancillary systems for large acceptance devices [22, 23] or magnetic spectrometers [18, 24]. Such detectors have the advantage of high angular segmentation, high energy resolution and a high degree of modularity. In this paper, we exploit the new modular device OSCAR [25] to investigate the one-proton transfer reaction ^{32}S(^{3}He,d)^{33}Cl at 9.8 MeV incident energy. This reaction is particularly suited to probe the spectroscopy (i.e. energy, J^{π} and C^2S_p spectroscopic factors) of low-lying states of the residual proton-rich ^{33}Cl nucleus by comparing measured differential cross section angular distributions with the predictions of theoretical calculations [26, 27]. However, while such theoretical predictions reached a level of good consistency, from the experimental point of view several ambiguities are still affecting the spectroscopy of ^{33}Cl low lying states, concerning especially J^{π} assignments and C^2S_p spectroscopic factors [28]. Such ambiguities arise especially from the presence of contaminants in the observed reaction products spectra that make it difficult to extract the differential cross section angular distributions in wide angular regions [29]. To improve previous studies of the ^{32}S(^{3}He,d)^{33}Cl reactions [30, 31], an essential ingredient is therefore to reduce possible sources of contaminants produced by undesired elements in the target and, additionally, to improve energy and angular resolution to more effectively disentangle the background from the signals to measure. Finally, a reliable measurement of the absolute cross-section scale is mandatory for a reasonable estimate of the C^2S_p factors.

2. Experimental setup

The experiment has been performed at the INFN-Laboratori Nazionali di Legnaro (LNL), Italy. A $^{3}He^{++}$ beam was delivered by the CN accelerator at an energy of 9.8 MeV on a 53 $\mu g/cm^2$ $^{nat}Zn^{32}S$ target, 99% enriched in ^{32}S. The $^{nat}Zn^{32}S$ powder is evaporated by electron beam technique on a thin substrate of carbon ($\approx$ 15 $\mu g/cm^2$) to reduce contaminant reactions. The target was installed in the center of a circular scattering chamber, shown in Figure 1. A rotating plate hosted two silicon telescopes, each constituted by an ORTEC surface barrier silicon followed by a high resolution Hamamatsu PIN diode, and an OSCAR telescope [25], placed on the opposite side of the beam line as shown in Figure 1. Both detectors have 2 detection stages to enable the particle identification via the ΔE-E technique. The OSCAR telescope was composed by a thin ($\approx$ 20 μm) 16-strips Single-Side Silicon Strip Detector (SSSSD) manufactured by Micron Semiconductors used as the first detection stage, and 16 individual silicon PIN diode pads (300 μm thick) manufactured by Hamamatsu used as the second detection stage. Each strip of the first detection stage is a 3.125 mm wide vertical silicon strip, while the silicon pads used as the second detection stage have an active area of 1 cm^2 and a ceramic frame of 1.4 mm and 3.2 mm on the bottom side. Each pad is installed on an electronic board containing plug-in pre-amplifiers, as discussed in [25] more in detail, while for the first detection stage we used a dedicated 16 channels pre-amplifier which lies below the rotating plate in Figure 1.

To determine the angular position of each detector with respect to the beam line we performed a dedicated measurement using an optical alignment telescope. Each of the measured positions is determined with an accuracy better than 0.2°. The optical alignment procedure allowed us also to benchmark the geometry information of the SSSSD detector claimed by the manufacturer. In the OSCAR hodoscope, the correlations between the first and second detection stages can be used to constrain with high precision the impact point on the surface of the detector and

IOP Conf. Series: Journal of Physics: Conf. Series **1308** (2019) 012007 doi:10.1088/1742-6596/1308/1/012007

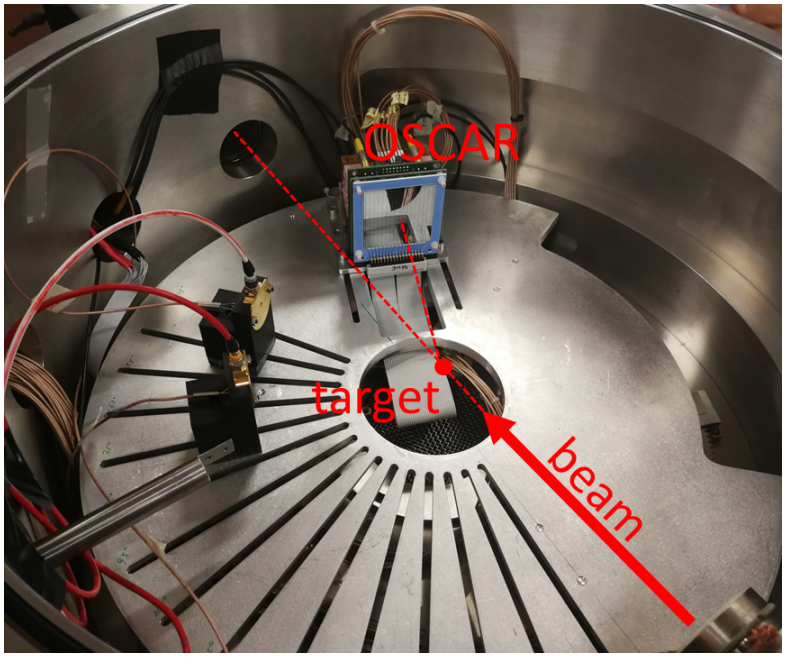

Figure 1. A photography of the experimental setup used for the experiment at INFN-LNL. The OSCAR hodoscope is installed at about 12 cm from the target in a circular vacuum chamber available in the experimental hall of the 5.5 MV CN accelerator. Other two individual telescopes were additionally installed. The rotating plate allows to easily change the laboratory angles of each detector.

therefore the emission angle of the particle emitted from the target. We define 64 individual pseudo-telescopes, each identified by the correspondence of a particular strip of the SSSSD with a pad in the second detection stage. This method allows to have 64 detection telescopes using only 32 individual electronics channels. The detection angle associated to each pseudo-telescope is defined as the geometrical center of the corresponding strip-pad correspondence. These are calculated with a Monte Carlo tool, starting from the absolute position of the OSCAR hodoscope measured with the optical telescope. In the procedure we generate random directions of incidence in the OSCAR telescope and then calculate the azimuthal and polar angle center of each pseudo-telescope from the corresponding distributions. Effective solid angles of each pseudo-telescope were benchmarked by means of a dedicated Monte Carlo tool as described in Ref. [25]. During the experiment, we used two different position of OSCAR in order to cover a larger region of detection angles, improved with respect to the state-of-the-art literature [30, 31]. In the first of the two geometry positions, OSCAR covered the laboratory angles from about $\theta = 20°$ to about $\theta = 40°$, while in the second the laboratory angles from $\theta = 40°$ to $\theta = 60°$ are covered. The overall coverage of the cumulative data is shown in Figure 3 in a deuteron energy vs θ plot.

3. Status of the data analysis

Particles in the OSCAR hodoscope are reconstructed by correlating strips in the first detection stage with pads in the second detection stage, according to the algorithm described in Ref. [25]. The energy deposited in the detector is calibrated independently for the first and the second stage by using the elastic scattering ^{3}He $+^{197}$ Au at 13 different incident energies, collected at the end of the experimental run. To account for small electronic drift effects affecting the

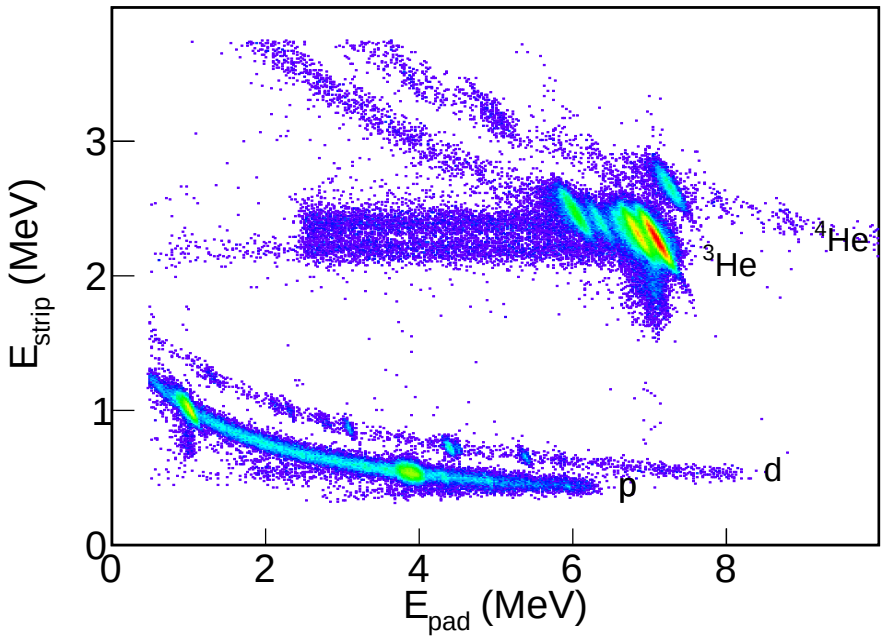

Figure 2. Experimental ΔE-E scatter plot for one of the pseudo-telescope of the OSCAR device. Both axes are calibrated in MeV. Different identification lines are identified by labels. Bumps observed on the deuteron line are produced by (^{3}He,d) on ^{32}S and the contaminants ^{12}C and ^{16}O.

quality of the energy calibration while merging data collected at different times during the experiment, we have produced a correction factor for each pseudo-telescope and each different run of the experiment. This procedure allows to maximize the statistics on the recorded spectra by maintaining an excellent energy resolution.

The particle identification is obtained by means of the ΔE-E identification technique, using the signals produced by the first (E_{strip}) and the second (E_{pad}) detection stages within a pseudo-telescope. Figure 2 shows a typical ΔE-E plot of a pseudo-telescope. Loci corresponding to protons, deuterons, ^{3}He and ^{4}He are clearly identified, as indicated by labels. We use a graphical cut procedure to unambiguously identify particles. Bumps lying on the observed ΔE-E loci are produced mainly by the occurrence of binary nuclear processes, such as scattering or binary reactions. Particularly interesting is the case of the deuteron locus, for which several bumps are well visible with a small background level, indicating the emission of deuterons from (^{3}He,d) transfer reactions. In the following analysis process, we will focus exclusively on well-identified deuterons.

In order to properly disentangle various (^{3}He,d) reactions induced on our target, we studied the kinematic lines associated to well-reconstructed deuterons in OSCAR. This is an advantage, with respect to previous investigations, introduced by the use of a new generation hodoscope, where many detection angles are achieved within the same geometry configuration. Figure 3 shows the deuteron kinetic energy as a function of the detection angle (θ) deduced with the procedure described above. The figure is produced by summing together data from 128 pseudo-telescopes, 64 for each of the two geometry configuration used during the experiment, covering

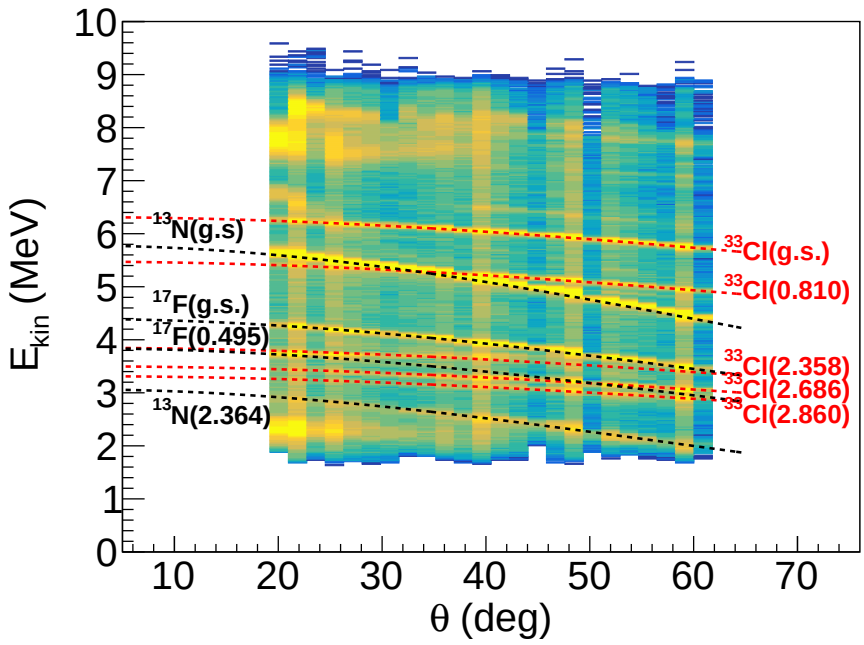

Figure 3. Experimental deuteron kinematic lines E_{kin} vs θ in the laboratory frame obtained with the OSCAR hodoscope and merging data from both the geometry configurations used in the experiment. Black and red dashed lines show the calculated kinematic lines respectively for contaminant reactions and ^{32}S(^{3}He,d)^{33}Cl reactions. ^{12}C and ^{16}O contaminants in the target are responsible for ^{13}N and ^{17}F residual nuclei lines, respectively.

a region of polar angles $20° \leq \theta \leq 60°$ in the laboratory frame. Several lines are clearly visible in the figure, indicating different (^{3}He,d) reactions. Red dashed lines are the result of our calculation assuming that the deuterons are emitted from the ^{32}S(^{3}He,d)^{33}Cl reactions, for different excitation energy states of the residual ^{33}Cl nucleus, indicated by labels. Black dashed lines are concurrent (^{3}He,d) reactions occurring on ^{12}C and ^{16}O contaminants present in the target backing. The latter give respectively ^{13}N and ^{17}F as the residual nuclei. In our calculation we take into account the energy loss by the beam in the target before reacting, assuming that the reaction occurs at mid target, and the energy loss by the emitted deuteron inside the target. Calculated lines are in excellent agreement with the observed ones, indicating the good consistency of our kinematics assumptions. In all the angular regions where the lines don't significantly overlap we can extract the yield of the ^{32}S(^{3}He,d)^{33}Cl reactions unambiguously.

The angular range shown in Figure 3 is segmented into angular regions according to the recorded statistics and to minimize the θ overlap between pseudo-telescopes of contiguous regions. We obtain over 30 separated angular regions. Within each region, we performed a multi-gaussian fit of the recorded peaks in the deuteron E_{kin} spectrum, according to the findings of Figure 3. In order to achieve a good consistency of the fit, we perform a simultaneous fit of data by using a function which contains the sum of all the gaussians. A typical example of such fits is shown in Figure 4, where the red line is the result of the fit. The fit reproduces well the overall shape of data. Peaks corresponding to the different reactions occurring on our ^{nat}Zn^{32}S target and the contaminant elements are identified by labels. The figure shows data

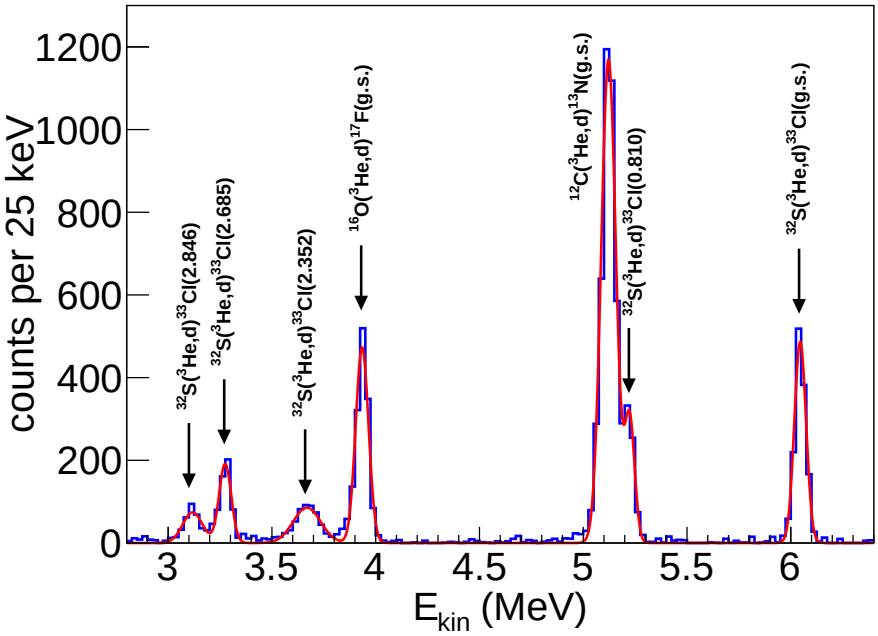

Figure 4. Experimental deuteron energy spectrum measured at $\theta \approx 40°$ with the OSCAR hodoscope. Data is obtained by merging 4 pseudo-telescopes. The red line is the result of a simultaneous fit of the spectrum with the superposition of gaussians to reproduce the observed peaks. Reactions responsible for each of the observed peaks are identified by labels.

within an angular slice centered at about $\theta = 40°$. The contribution of ^{32}S(^{3}He,d)^{33}Cl reactions leaving the residual ^{33}Cl in its ground state, the 2.352 MeV, the 2.685 MeV and the 2.846 MeV states are clearly visible, well separated from the contaminant peaks, as expected from the results shown in Figure 3. The ^{16}O(^{3}He,d)^{17}F(0.495) peak is strongly suppressed at this angle, and its contribution to the high energy tail of the ^{32}S(^{3}He,d)^{33}Cl(2.686) is negligible. The ^{32}S(^{3}He,d)^{33}Cl(0.810) is partially overlapped with the prominent ^{12}C(^{3}He,d)^{13}Cl(g.s.) peak, because of the kinematics, but, thanks to the excellent resolution of our apparatus, we are able to resolve both yields. The latter is particularly important at all angles, representing the major contaminant in our investigation, and making it extremely difficult to extract the yield of the ^{32}S(^{3}He,d)^{33}Cl(0.810) reaction in the angular region $25° \leq \theta \leq 35°$. However, at angles greater than $\approx 40°$ the separation in energy of these reactions is sufficiently large to allow an easy separation of the corresponding yields.

Finally, to extract the absolute cross-section of each of the measured ^{32}S(^{3}He,d)^{33}Cl reactions, we reduced indeterminations arising from the target thickness and the beam charge integration by internal normalization to the ^{3}He + Zn Rutherford scattering. The latter appears as a prominent peak in the ^{3}He kinetic energy spectra, well visible at all angles.

4. Conclusions and Perspectives

To try to solve the ambiguities in the experimental knowledge of low-lying states in the proton-rich ^{33}Cl nucleus, we have performed an investigation of the ^{32}S(^{3}He,d)^{33}Cl one-proton transfer reaction by using the new generation hodoscope OSCAR. The combination of the excellent

energy resolution, the particle identification capabilities and the presence of several detection angles allow us to firmly extract the yield of ^{32}S(^{3}He,d)^{33}Cl reactions over the background caused by contaminants, in a wide angular domain $20° \leq \theta \leq 60°$. We are able to extract the yield of ^{32}S(^{3}He,d)^{33}Cl reactions leaving the ^{33}Cl residual nucleus in the ground state and in its 0.810 MeV, 2.352 MeV, 2.685 MeV, 2.846 MeV excited states. The absolute differential cross-sections will be deduced by normalization to the ^{3}He + Zn Rutherford scattering, thus removing any additional uncertainty related to the thickness of the target and the beam charge integration.

Our new data will be compared with the state-of-the-art shell model calculations used to describe nuclei in the (s-d)-shell to refine our knowledge of the spectroscopy of the observed states, including J^{π} values and the C^2S_p spectroscopic factors.

5. Acknowledgments

We acknowledge M. Loriggiola of the INFN-LNL Target Laboratory (Servizio Utenti) for manufacturing and characterizing extremely high quality and low contaminants targets. We are thankful to the staff of the CN accelerator of the INFN-LNL for producing and delivering the high-quality beams used for the experiment.

References

[1] Lombardo I *et al.* 2014 *Bulletin of the Russian Academy of Sciences: Physics* **78** 1093
[2] Lombardo I *et al.* 2014 *J. Phys. Conf. Ser.* **569** 012068
[3] Lombardo I, Dell'Aquila D, Spadaccini G, Verde G and Vigilante M 2018 *Phys. Rev. C* **97**(3) 034320 URL `https://link.aps.org/doi/10.1103/PhysRevC.97.034320`
[4] He J J *et al.* 2018 *Chin. Phys. C* **42** 15001
[5] Dell'Aquila D 2016 *Il Nuov. Cim. C* **39** 272
[6] Dell'Aquila D *et al.* 2017 *Phys. Rev. Lett.* **119** 132501
[7] Lombardo I *et al.* 2016 *J. Phys. G.* **43** 45109
[8] Spitaleri C *et al.* 2017 *Phys. Rev.* **C95** 035801
[9] Piantelli S *et al.* 2017 *Phys. Rev. C* **96** 034622
[10] Borderie B *et al.* 2018 *Phys. Lett. B* **782** 291
[11] DeFilippo E *et al.* 2009 *Acta. Phys. Pol. B* **40** 1199
[12] Morelli L *et al.* 2016 *J. Phys. G: Nucl. Part. Phys.* **43** 045110
[13] Russotto P *et al.* 2015 *Phys. Rev. C* **91** 014610
[14] Lombardo I *et al.* 2010 *Nucl. Phys. A* **834** 458c
[15] Pastore G *et al.* 2017 *Nucl. Instr. Meth. Phys. Res. A* **860** 42
[16] Lombardo I *et al.* 2013 *Nucl. Instr. Meth. Phys. Res. B* **302** 19
[17] Cappuzzello F *et al.* 2016 *Eur. Phys. J. A* **52** 167
[18] Fernández-Domínguez B *et al.* 2011 *Phys. Rev. C* **84** 011301
[19] Nevelinga R *et al.* 2011 *Nucl. Instr. Meth. Phys. Res. A* **654** 29
[20] Acosta L *et al.* 2016 *J. Phys. Conf. Ser.* **730** 012001
[21] Dell'Aquila D *et al.* 2019 *Nucl. Instr. Meth. Phys. Res. A* **929** 162
[22] Cardella G *et al.* 2015 *Nucl. Instr. Meth. Phys. Res. A* **799** 64
[23] Martorana N *et al.* 2018 *Phys. Lett. B* **782** 112
[24] Adsley P *et al.* 2017 *JINST* **12** T02004
[25] Dell'Aquila D *et al.* 2018 *Nucl. Instr. Meth. Phys. Res. A* **877** 227
[26] Wildenthal B *et al.* 1971 *Phys. Rev. C* **4** 1708
[27] Castel B *et al.* 1971 *Nucl. Phys. A* **162** 273
[28] Chen J and Sing B 2011 *Nucl. Data Sheets* **112** 1393
[29] Elbakr S *et al.* 1971 *Can. J. Phys.* **50** 674
[30] Kozub R and Youngblood D 1972 *Phys. Rev. C* **5** 413
[31] Inglima G *et al.* 1975 *Nuov. Cim. A* **26** 211